Cold ion–polar-molecule reactions studied with a combined Stark-velocity-filter–ion-trap apparatus

Kunihiro Okada,[1,*] Takuya Suganuma,[1] Takahiro Furukawa,[1] Toshinobu Takayanagi,[1]
Michiharu Wada,[2] and Hans A. Schuessler[3]

[1]*Department of Physics, Sophia University, 7-1 Kioicho, Chiyoda, Tokyo 102-8554, Japan*
[2]*RIKEN Nishina Center for Accelerator-Based Science, 2-1 Hirosawa, Wako, Saitama 351-0198, Japan*
[3]*Department of Physics, Texas A&M University, College Station, Texas 77843, USA*

(Received 22 January 2013; revised manuscript received 9 April 2013; published 26 April 2013)

We have developed a combined Stark-velocity-filter–ion-trap apparatus for the purpose of reaction-rate measurements between cold trapped ions and slow polar molecules under ultrahigh vacuum conditions. The prerequisite steps such as the characterization of velocity-selected polar molecules (PM), namely ND_3, H_2CO, and CH_3CN, were performed using time-of-flight (TOF) measurements. We confirmed the generation of slow ND_3, H_2CO, and CH_3CN molecules having thermal energies of a few Kelvin. Additionally, the number densities of the slow velocity-filtered polar molecules were determined to be in the range of $n = 10^4$ to 10^6 cm^{-3} by calibrating the TOF signals. In a first experiment, the Stark velocity filter was connected to a cryogenic linear Paul trap and reaction-rate measurements between laser-cooled Ca^+ Coulomb crystals and velocity-selected polar molecules were carried out. The observed reaction rates are of the order of 10^{-5} s^{-1}, which are much slower than typical reaction rates of molecular ion–polar-molecule reactions at low temperatures. The present results confirm that reaction-rate measurements between velocity-selected polar molecules and sympathetically cooled molecular ions cooled by a laser-cooled Ca^+ Coulomb crystal can be performed. Next we measured the reaction rates between sympathetically cooled nonfluorescent stored ion molecules namely N_2H^+ ions and velocity-selected CH_3CN molecules at the average reaction energy of about 3 K. The measured reaction rate of $2.0(2)\times10^{-3}$ s^{-1} is much faster than those of the $Ca^+ + PM$ reactions. This is strong evidence that the velocity-selected polar molecules undergo reactive collisions. We also confirmed that the present reaction-rate constant of $CH_3CN + N_2H^+ \rightarrow CH_3CNH^+ + N_2$ is consistent with the estimated values from the room temperature results and the trajectory-scaling formula of Su *et al*. In the future, the present velocity-filter combined cryogenic trap apparatus will enable us to perform systematic measurements of cold ion–polar-molecule reactions, which are important problems from a fundamental viewpoint and also contribute to astrochemistry.

DOI: 10.1103/PhysRevA.87.043427 PACS number(s): 37.10.Ty, 37.10.Rs, 82.30.Fi, 52.27.Jt

I. INTRODUCTION

Cold molecules and their ions are attractive research objects in the fields of fundamental physics and cold chemistry. In connection with the cold chemistry, cold ion-molecule reactions play important roles in the synthesis of interstellar molecules because their reaction-rate constants are important information for studying the chemical evolution of interstellar clouds [1]. Therefore, databases of the rate constants have been developed for astrochemistry and some reaction network models were proposed to understand the synthetic mechanisms of interstellar molecules [2,3]. Recently, the present state of knowledge concerning the reaction-rate constants and their uncertainties for the major gas-phase chemical processes was reviewed [4]. It was pointed out that most of the measurements of ion-neutral reactions were only performed at room temperature or in a restricted range of temperatures near room temperature, even though the reactions occur at low temperatures in interstellar clouds. Especially, cold ion–polar-molecule reactions have not been studied extensively in the laboratory owing to experimental difficulties, such as the condensation or sublimation of polar gases at low temperatures. The data at low temperatures are usually estimated from extrapolation values of room temperature results [4], or using the trajectory-scaling formula [5]. For that reason, we planned to experimentally determine the reaction rates between cold molecular ions and polar molecules using the ion-trap technique. The final goal of the present study is to provide required information for cold chemistry in interstellar clouds and contribute to the astronomical databases.

At present, various techniques producing cold neutral molecules have been established. A technique for preparing state-selected molecular targets using unimolecular reactions with laser fields or bimolecular reactions between state-selected reaction partners were demonstrated [6,7]. The main goal in these studies is to perform cold controlled chemistry. A Stark decelerator is also used to produce cold polar molecules with optimized energy resolution [8]. As an interesting application of the decelerator, crossed molecular beam scattering experiments between decelerated polar molecules and rare-gas atoms have been performed [9]. A simple and powerful method to produce slow polar molecules is Stark velocity filtering, which was developed by several groups [10,11]. The method exploits the fact that a large quantity of slow polar molecules is always existing on the low velocity side of the Maxwell-Boltzmann velocity distribution of thermal gases even at room temperature. Slow molecular beams with a translational temperature of a few Kelvin are readily available using this technique [12]. Recently, a new method to directly measure cold ion–polar-molecule reactions at very low pressure was demonstrated by combining a laser-cooling technique with a Stark velocity filter [13]. In the experiment, the reaction rate between a Ca^+ Coulomb crystal and velocity-selected CH_3F molecules was measured at about 1 K. We plan to

*okada-k@sophia.ac.jp

 ©2013 American Physical Society

extend this kind of experiment to reaction-rate measurements between stored *sympathetically* cooled molecular ions and velocity-selected slow polar molecules. The sympathetic cooling technique is applicable to a wide variety of molecular ions.

In this paper, we report on the development of a setup consisting of a Stark velocity filter and a cryogenic linear Paul trap for the purpose of reaction-rate measurements of cold molecular ion–polar-molecule reactions. In addition, the results of the reaction-rate measurements are reported. The paper is organized as follows. An overview of the working of the Stark velocity filter and the cryogenic linear Paul trap is described in Sec. II. In Sec. III, the characterization of the Stark velocity filter is performed by measuring the intensity and the velocity distribution of slow polar molecules in a time-of-flight (TOF) experiment. In Sec. IV, we describe a numerical simulation of the velocity filtering in order to obtain the information for the velocity distributions, the rotational state distribution, and the spatial divergence of a molecular beam after passing through the beam-guide exit. The results of the reaction-rate measurements of cold ion–polar-molecule reactions are presented in Sec. V. Finally we summarize the results in Sec. VI.

II. EXPERIMENTAL SETUP

The experimental setup is shown in Figs. 1(a)–1(d). The setup consists of a Stark velocity filter and a detection vacuum chamber enclosing a cryogenic linear rf ion trap. The vacuum chamber for the Stark velocity filter is made of an aluminum alloy, and was fabricated by ethanol lathing. The chamber is divided into two parts for differential pumping. The background pressures of the first and second chambers are kept at about 10^{-4} Pa and 10^{-6} Pa during reaction-rate measurements. As shown in the insert of Fig. 1(b), the molecular beam guide consists of four stainless steel rods with a diameter of 2 mm and the distance between the rods is designed to be 1 mm [10]. The radii of the curvature of the first and second bent sections are 12.5 mm and 25 mm, respectively, and the total length of the beam guide is 942 mm. In the present setup, the maximum guiding voltages V_G applied to the quadrupole electrodes is ± 3.0 kV, which corresponds to the nominal electric field of 60 kV/cm. In fact, the maximum electric field is possibly somewhat higher due to imperfections of the arrangement of the guide electrodes, as is described in Sec. IV. From the gas inlet, a polar gas is loaded into a ceramic nozzle with an inner diameter of 1.5 mm. The gas nozzle, if needed, is cooled by a cryocooler in order to increase the intensity of the slow polar molecules. For thermalization of a loaded polar gas, a stainless steel pipe with a 3 mm diameter is plugged in a copper block, which is about 14 cm long and is thermally contacted to the cold head of the cryocooler. The nozzle temperature is variable from room temperature to 50 K by simultaneously driving the cryocooler and ceramic heaters, which are fixed to the nozzle mount. The nozzle temperature is monitored by a silicon-diode sensor.

We generated slow polar molecules of CH_3CN, ND_3, and H_2CO, which are commercially supplied as a liquid (CH_3CN), a gas (ND_3), and a powder (paraformaldehyde). For the experiment of CH_3CN, the liquid sample of CH_3CN is prepared in a reservoir made of Pyrex glass, which is connected to a vacuum system. In order to remove impurities in the liquid sample, we repeated a standard purification procedure (freezing by liquid-nitrogen, evacuating and melting) many times. Then, we introduce the polar gas through the variable leak valve, which is heated by a sheathed heater to avoid clogging of the valve. On the other hand, the powder sample of paraformaldehyde is put in a stainless tube. Then, we heat the tube and the valve to 70 °C by a sheathed heater. The absolute pressure of polar gases is monitored by a capacitance manometer (Baratron, Type 127, 1 Torr full scale). Typically, the nozzle pressure is set to 30–40 mTorr in order to obtain a maximum signal of velocity-selected molecules.

Figure 1(d) shows the photograph of the detection vacuum chamber containing a linear Paul trap. During the reaction experiments the base pressure is maintained to be less than 10^{-8} Pa. The linear Paul trap consists of four segmented stainless steel rods with a diameter of 8 mm and the inner radius (r_0) is 3.5 mm. The driving frequency and the amplitude of the trap are typically 4.87 MHz and 130 V, respectively. In this case, the pseudopotential for Ca^+ ions is about 0.89 eV in the radial direction. The base plate of the linear ion trap is cooled by a liquid nitrogen baffle to reduce background gases. In particular this cryogenic linear trap is indispensable to avoid undesirable reactions between cold ions and stray polar molecules, which are possibly leaked from upstream of the Stark velocity filter.

We equipped the setup with an electron gun for producing molecular ions by electron impact ionization. For the sympathetic laser cooling of molecular ions, Ca^+ ions are produced and trapped by the laser-ablation method [14], and laser cooled. The ion trap is divided into two sections in order to avoid contamination on the electrodes by the ablated atoms; one section is the initial loading area by laser ablation and the other one is the spectroscopy section. The length of the spectroscopy section is 10 mm along the trap axis. The distance between the beam-guide exit and the trap section is 33 mm.

Since a detailed description of the laser system and the fluorescence detection system is given in the previous paper [15], it suffices to briefly explain the setup as follows. For laser cooling of trapped Ca^+ ions, we used two grating-stabilized diode lasers with wavelengths of 397 nm and 866 nm, which are frequency stabilized by a stable helium-neon laser through transfer cavities. The laser beams are incident along the linear trap axis in a collinear arrangement. The laser-induced fluorescence (LIF) image of Ca^+ ions is observed by a cooled CCD camera with a $\times 10$ or $\times 6$ magnification telecentric lens system at right angles to the trap axis. Since the magnification of the detection optics is known, we can determine the size of the Ca^+ Coulomb crystal from the observed fluorescence image. In this way the relative number of Ca^+ ions is determined with the assumption of a constant number density of cold Ca^+ ions.

III. CHARACTERIZATION OF VELOCITY-SELECTED POLAR MOLECULES

A. Velocity distribution

In order to characterize the Stark velocity filter, we performed TOF measurements for the velocity-selected

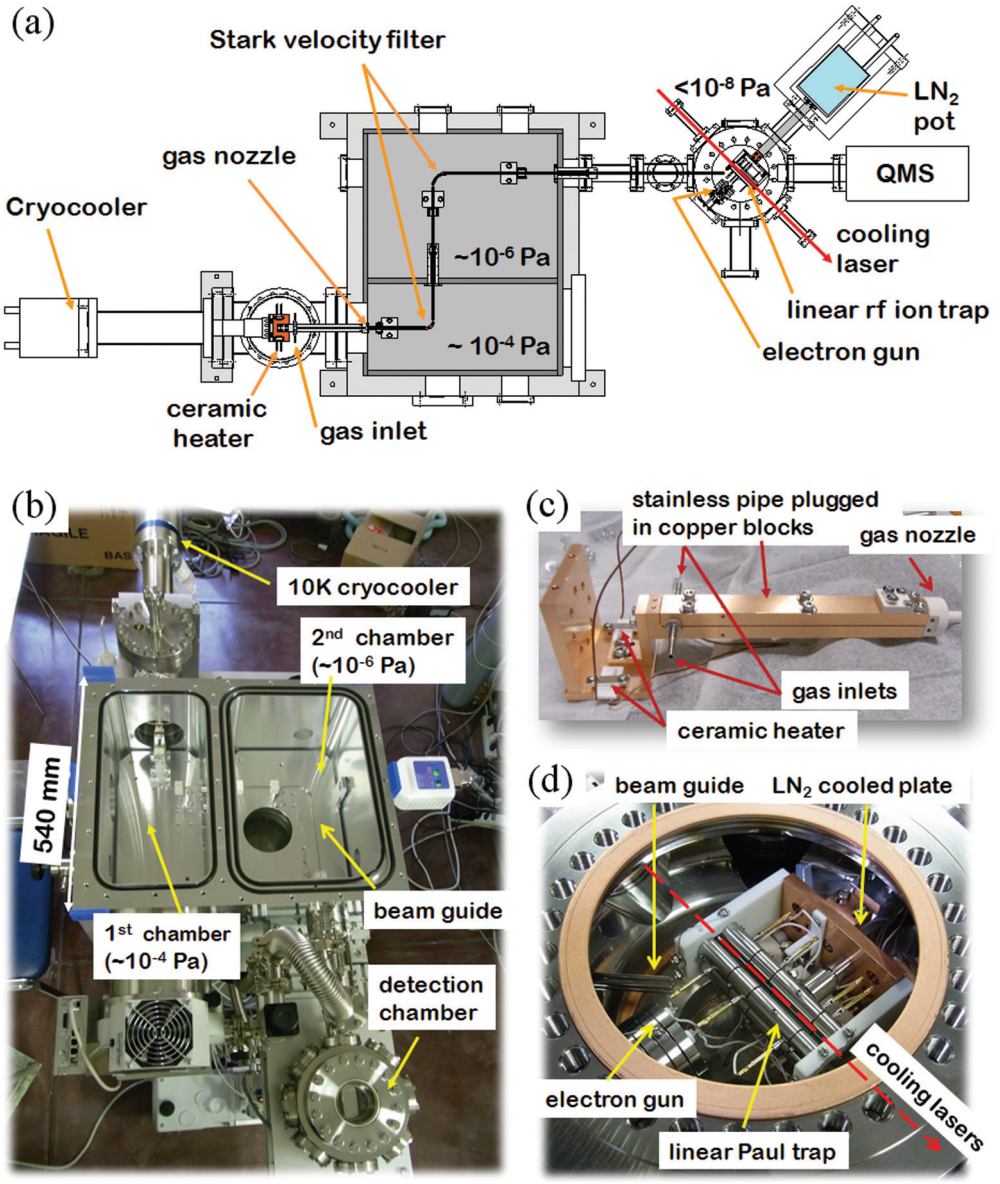

FIG. 1. (Color online) (a) Schematic drawing of the experimental setup. (b) A photograph of the vacuum chamber enclosing the Stark velocity filter. The vacuum chamber is made of aluminum alloy and is divided into two chambers to establish a differential pumped system. (c) Details of the gas nozzle assembly. The nozzle with a diameter of 1.5 mm is made of a ceramic material to avoid a discharge between the nozzle and the quadrupole electrodes. For thermalization of an introduced polar gas, the stainless steel pipe with a 3 mm diameter is plugged in a copper block, which is thermally contacted to the cold head of the 10 K cryocooler. A silicon-diode sensor is mounted on the nozzle to monitor the gas-nozzle temperature. (d) A photograph of a detection vacuum chamber containing a cryogenic linear Paul trap.

polar molecules. The velocity distributions of the slow polar molecules were extracted from the TOF signals. To begin with, we placed a quadrupole mass spectrometer (QMS) (Stanford Research, RGA100) in front of the beam-guide exit to measure the TOF signals of slow polar molecules. Using a high-voltage solid-state switch, the guiding voltages of the Stark velocity filter were quickly turned on (∼10 ns/kV). The repetition frequency of the switch is 5–10 Hz with a 50% duty cycle, and the number of the switching cycles for observation is typically 5000.

Figure 2(a) shows the TOF signals of slow polar molecules (CH_3CN, H_2CO, ND_3) at several different guiding voltages. In these measurements, the singly ionized molecular ions were detected by a secondary electron multiplier at the end of the QMS. At $t = 0$, the guiding voltages were quickly turned on. The QMS signal starts rising after about 10–20 ms and a steady state of the molecular beam intensity is reached. Since the maximum cutoff velocity of the guided molecules in the Stark velocity filter is determined by both the guiding voltages as well as the radius of curvature of the bent section of the beam guide, the rise time of the growth curves and the intensity at the steady state strongly depend on the guiding voltages.

The time differentiation of the time-distribution signals $I(t)$ yields the velocity distributions, where the Gompertz function, that is $\exp\{-\exp[-k(t - t_c)]\}$, was used to reproduce the

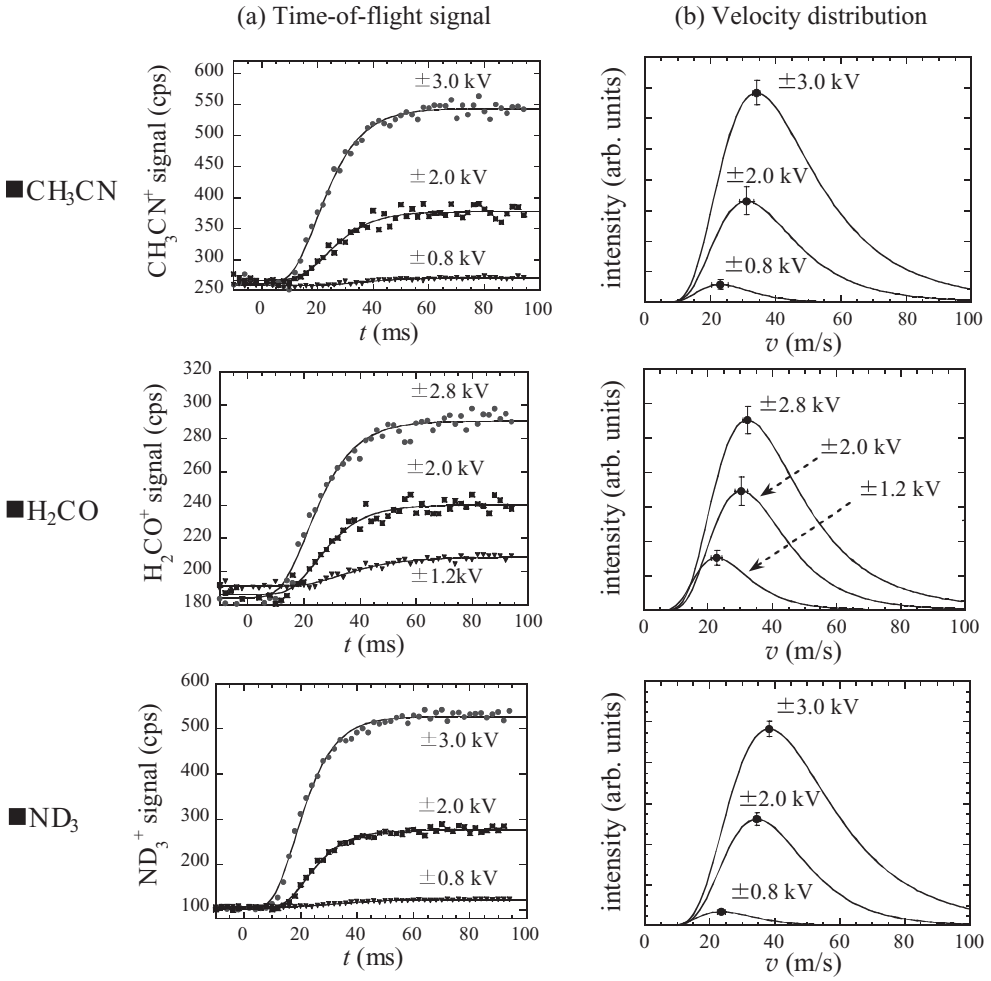

FIG. 2. (a) Time-of-flight (TOF) signals of guided polar molecules at different guiding voltages. The solid lines show the fitted curve of the Gompertz function to the experimental data points. (b) The velocity distributions derived from the TOF signals. The representative errors are shown at the peak positions. In these experiments, room temperature polar gases were introduced. The nozzle pressures of CH_3CN, ND_3 and H_2CO are set to 32, 40, and 41 mTorr, respectively.

experimental growth signals [16]. Figure 2(b) shows the velocity distributions derived from the TOF signals using the following equation:

$$f(v) = \frac{l}{v^2}\left(\frac{dI(t)}{dt}\right). \quad (1)$$

Here l is the flight distance of the guided polar molecules between the nozzle and the detector.

As shown in Fig. 2(b), the peak velocity, v_p, decreases as the guide voltage decreases. At the guiding voltage of ± 0.8 kV, v_p corresponds to a thermal energy of only 1.3 K for the CH_3CN measurement. The same measurements for ND_3 and H_2CO molecules were also performed and show that slow polar molecules with a thermal energy of less than 3 K were successfully produced (see Table I).

B. Nozzle temperature and pressure dependence

For the ND_3 gas the TOF measurement was performed at lower nozzle temperatures by simultaneously driving the cryocooler and the ceramic heater. Since the condensation

TABLE I. Summary of the characterization of the velocity-selected polar molecules. v_p is the peak velocity in the longitudinal velocity distribution, which was determined by the TOF measurement. T_p represents the thermal energy, which is estimated by the relation of $mv_p^2/2 = k_B T_p$. T_{1D} is the estimated longitudinal temperature from the most probable velocity of the one-dimensional thermal velocity distribution fitted to the simulation results (see Sec. IV B). n is the experimentally determined number density of slow polar molecules at the position of the ion trap. The error in the parenthesis includes the statistical error and the uncertainty of the ionization pressure gauge (16%). The simulated systematic error due to the spatial divergence of the guided molecules after passing through the beam guide exit is not included (see Sec. IV C). The last column shows the nominal guiding voltages (V_G) applied to the quadrupole electrodes.

Molecule	v_p (m/s)	T_p (K)	T_{1D} (K)	n (cm^{-3})	V_G (kV)
CH_3CN	34(1)	2.9	6.4	$1.2(0.3) \times 10^5$	±3.0
ND_3	38.4(0.9)	1.6	5.1	$8.5(1.9) \times 10^5$	±3.0
H_2CO	32(1)	1.8	5.5	$1.4(0.3) \times 10^6$	±2.8

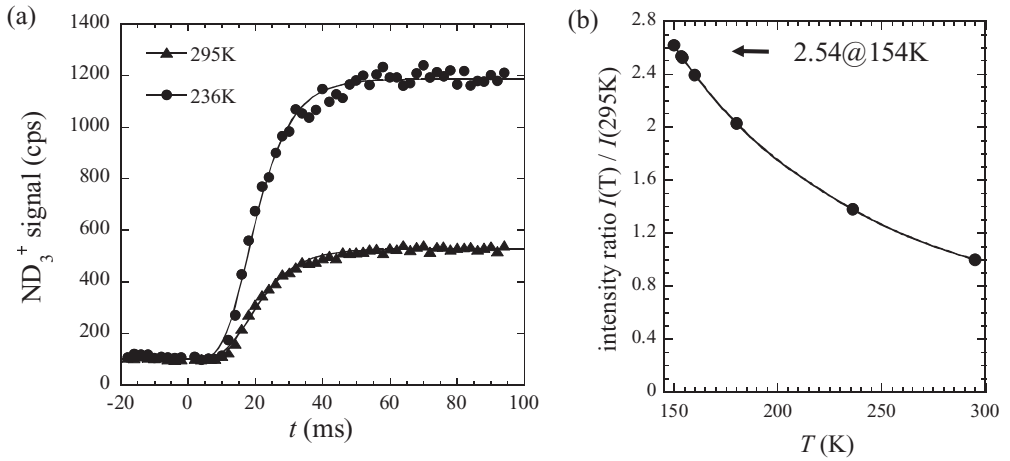

FIG. 3. (a) The TOF signals of the velocity-selected ND_3 molecules measured at the different nozzle temperatures of 295 and 236 K. The guiding voltages and the nozzle pressure are ±3.0 kV and 41 mTorr, respectively. (b) A plot of the integrated intensity ratio $I(T)/I(295\ \mathrm{K})$ of slow velocity components in the Maxwell-Boltzmann velocity distribution as a function of temperature. $I(T)$ is obtained by integrating the velocity distribution from $v = 0$ to 150 m/s.

of ND_3 gas is expected to occur at low temperatures, the nozzle temperature was optimized to obtain the highest signal intensity of the velocity-selected ND_3 molecules. As a result, we found about 236 K as the optimum nozzle temperature for the present experimental conditions. Below this nozzle temperature, although the TOF signal temporarily increases, it gradually decreases as time progresses. Figure 3(a) shows the TOF signals of the velocity-selected ND_3 at different nozzle temperatures of 295 and 236 K. As compared to the case of room temperature (295 K), the saturated signal intensity was increased about 2.5 times. Since this increase is caused by the increase of the slow velocity components in the Maxwell-Boltzmann velocity distribution, the integrated intensities of the slow velocity components were calculated to compare them to the experimental result. As shown in Fig. 3(b), the intensity at 236 K is too small to explain the increase of the signal in the present experiment. More likely the temperature of ND_3 gas at the nozzle is lower and is considered to have been about 154 K. This temperature is in good agreement with the previous study by another group [17].

We also measured the nozzle pressure dependence of the saturated signal intensity of the velocity-selected polar molecules. The detailed result for ND_3 molecules is shown in Fig. 4. The measurements were performed from 3 to 279 mTorr at a low nozzle temperature of 251 K. It is conceivable that the linear increase of the signal at lower pressure than about 20 mTorr is due to the increase of the molecular beam flux in molecular flow regime. Above 20 mTorr, the signal starts deviating from the linear dependence and it saturates at about 40 mTorr. Since the molecular flow regime gradually changes into viscous flow regime, the loss of the slow velocity components increases by the collisions with other polar molecules after 40 mTorr [17]. Then, the signal gradually decreases with increasing the pressure. This phenomenon was also confirmed by the change of the velocity distribution. Figure 4(b) shows a plot of the peak velocity as a function of nozzle pressure. The peak velocity gradually shifts to the higher velocity side due to the removal of the slow velocity components.

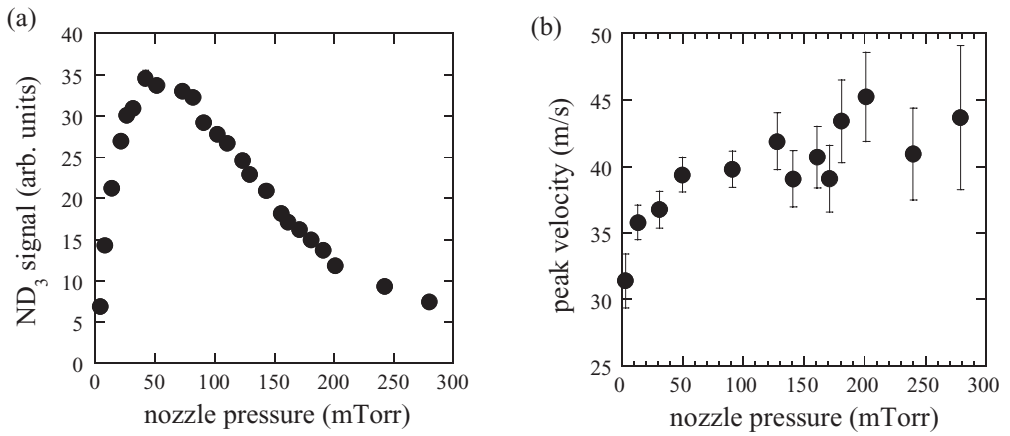

FIG. 4. (a) Nozzle pressure dependence of the guided ND_3 signal intensity measured by the TOF method. In this experiment, the guiding voltages of $V_G = \pm 2.4$ kV are applied. The nozzle temperature is set to 251 K. The error bar of each point is within the mark. (b) A plot of the peak velocity as a function of nozzle pressure. The peak velocity gradually increases with increasing the pressure.

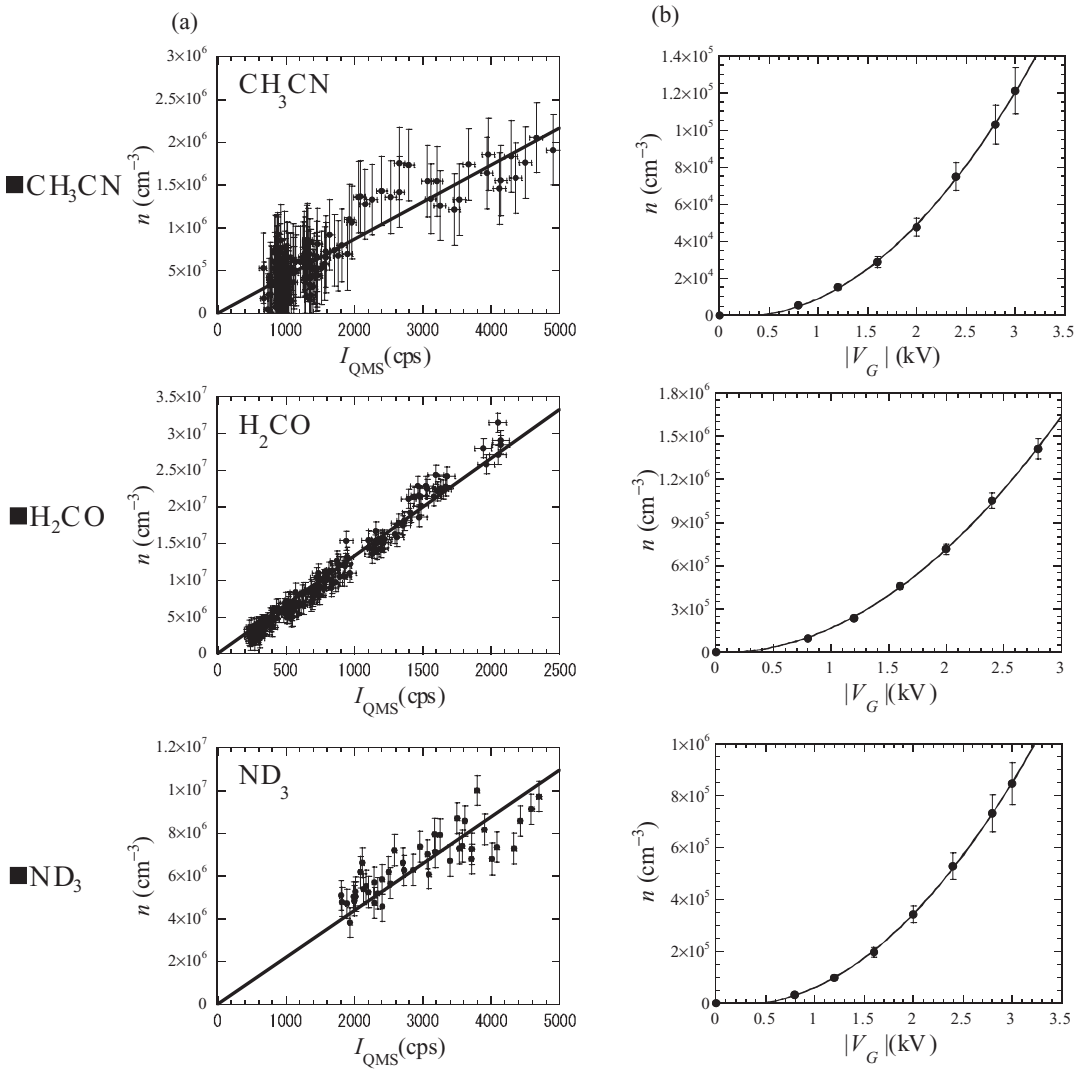

FIG. 5. (a) Examples of correlation plots for the number density (n) of polar molecules as a function of the ion-count signal (I_{QMS}) detected by the quadrupole mass spectrometer (QMS). The position of the ring filament in the ionization cage of the QMS was adjusted to 33 mm as measured from the beam-guide exit, which corresponds to the distance from the center of the linear Paul trap. We repeated the same measurement six to ten times in order to obtain the conversion factors from I_{QMS} to n (see the text). (b) A plot of the number density of the velocity-selected polar molecules as a function of the guiding voltage. The data points are calculated by Eq. (2) and the solid curve is the fitted function which is proportional to $|V_G|^2$ [10].

C. Determination of the number density

The number density of the velocity-selected polar molecules is a very important parameter to determine the reaction rate constants. The determination procedure is described as follows. First, the polar gas is loaded through a variable leak valve into the vacuum chamber containing the ion trap. When performing the TOF measurements, the position of the ring-shaped filament of the ionization cage of the QMS was adjusted to the same distance (33 mm) as between the linear Paul trap center and the beam-guide exit. Then we simultaneously measure the ion count signal I_{QMS} of the singly ionized polar molecules by the QMS and the pressure of the introduced polar gas by the ionization pressure gauge. In order to obtain the true polar-gas pressure, the measured pressure was corrected by multiplying with a correction factor, which is determined by the ratio between the electron-impact ionization cross sections of N_2 and of the respective polar molecules at 45 eV. We actually used 0.36 for CH_3CN, 0.915 for ND_3 and 0.55 for H_2CO as the correction factors [18–21]. Finally, we obtain a correlation plot between I_{QMS} and the number density (n) (Fig. 5). By a least-square fit of the linear function $n = \alpha I_{\mathrm{QMS}}$, the conversion relation was obtained. In the experiment we repeated the same measurement for six to ten times.

The final results of the conversion factors are summarized as follows:

$$\begin{aligned} n(\mathrm{CH_3CN}) &= 4.3(0.4) \times 10^2 I_{\mathrm{QMS}}, \\ n(\mathrm{H_2CO}) &= 1.33(0.07) \times 10^4 I_{\mathrm{QMS}}, \\ n(\mathrm{ND_3}) &= 2.0(0.1) \times 10^3 I_{\mathrm{QMS}}, \end{aligned} \tag{2}$$

where the unit of n is cm^{-3}. The error in the parenthesis is caused by the statistical error. As an example, the number

density of the velocity-selected CH_3CN molecules is determined to be 1.2(0.3) $\times$ 10^5 cm^{-3} at the guiding voltage of $\pm$3.0 kV. The error includes the statistical error and the uncertainty of the ionization pressure gauge, which is 16% according to the manufacturer data. The systematic error due to the spatial divergence of the guided molecules after passing through the beam guide exit is considered in Sec. IV C. The thermal energy of the velocity selected CH_3CN at $|V_G| = 3.0$ kV is estimated to be about 3 K by assuming the relation of $mv_p^2/2 = k_BT$. A summary of the experimental data taken by the Stark velocity filter is given in Table I.

IV. SIMULATION OF VELOCITY FILTERING

We have developed a Monte Carlo simulation code to characterize the present Stark velocity filter. On one hand, we obtain the information of the transverse velocity distribution, which cannot be measured experimentally in the present setup. On the other hand, the rotational state distribution of the velocity-selected polar molecules can be obtained. Finally, we can simulate the spatial divergence of the slow polar molecular beam after passing through the beam-guide exit. The information is used to evaluate the systematic error of the experimentally determined number density.

A. Method of calculation

Trajectories of polar molecules were obtained by performing the numerical integration of the equation of motions using the fourth-order Runge-Kutta algorithm. The initial positions of the input molecules were set within $\phi = 1$ mm by using uniform random numbers, and the initial velocities were randomly set according to the Maxwell-Boltzmann distribution at a given temperature. The rotational state distribution, calculated by $\exp[-E_{\rm rot}(J,K)/k_BT)]$, was considered as a weighting factor to the intensity of the transmitted polar molecules in the beam guide. We also took the degeneracy arising from nuclear spin statistics into account [22]. Since in the present setup the cutoff velocity of polar molecules along the beam-guide axis is determined by the first bent section with the curvature radius of $R = 12.5$ mm, we considered only the first bent section to calculate molecular trajectories (Fig. 6).

The quadrupole potential in the bent section of the beam guide is approximately expressed by the following equation for the geometry depicted in Fig. 6(b).

$$\phi_\theta(x,y,z) = \frac{\kappa_0 V_G}{r_0^2}\{(z\cos\theta + x\sin\theta - R)^2 - y^2\}, \quad (3)$$

where $\theta = \tan^{-1}(x/z)$. r_0 and R are the inner radius of the quadrupole guide and the radius of the curvature of the bending section in the beam guide, respectively. The equation for $\theta = 0$ and $\pi/2$ expresses the quadrupole potential in the yz and xy plane, respectively. κ_0 is the geometrical factor which is introduced for fitting the equation to the actual beam guide geometry. In the present simulation, the geometric factor κ_0 is set to 1.53. The electric fields at the specific position can be calculated by $\boldsymbol{E}(x,y,z) = -\nabla\phi_\theta$. The force acting on a polar molecule is determined by the Stark shift energy of each rotational state. The three-dimensional force on a polar molecule is calculated by $\boldsymbol{F} = -\nabla W_{\rm Stark}$, which is the Stark

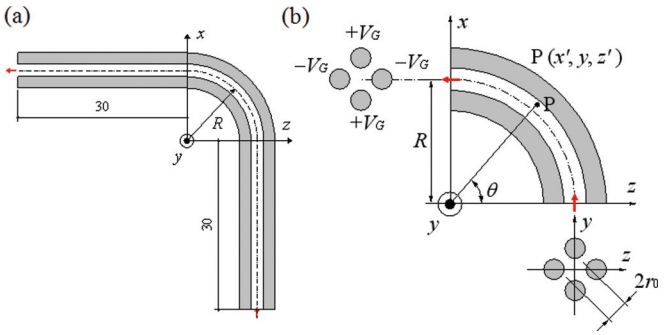

FIG. 6. (Color online) (a) The geometry of the quadrupole beam guide for the Monte Carlo simulation. The polar molecules randomly enter into the beam guide from the bottom ($x = -30, z = 12.5$). The initial positions of molecules within the diameter of 1.0 mm on the yz plane are determined by generating uniform random numbers. The initial velocities were randomly set according to the Maxwell-Boltzmann distribution at a given temperature. (b) An enlarged view of the first bent section of the beam guide for the simulation. The radius of the curvature is $R = 12.5$ mm. The electric potential on the $y'z'$ plane at an angle θ is expressed by $\phi(x,y,z) = V_G\{(z'-R)^2 - y'^2\}/r_0^2$, where $y' = -z\sin\theta + x\cos\theta$, $z' = z\cos\theta + x\sin\theta$.

shift energy at a certain position. For the fast numerical calculations, the field dependence of the Stark energy shifts of the rotational states are individually fitted to a fourth-order polynomial function in the electric field strength [23]. The fitted coefficients for all low-field-seeking states up to to the specified J were derived and stored in a text file. Then, we numerically solve the equations of motion for the input polar molecules, which are randomly generated as previously mentioned.

For ND_3, a typical trial number for the Monte Carlo simulation is 4 $\times$ 10^4 for each low-field-seeking state and the rotational states up to $J = 25$ are considered. On the other hand, we considered the rotational states up to $J = 50$ and 16 for CH_3CN and H_2CO, respectively. Finally, the position, the velocity and the relative population of each transmitted molecule with a specific rotational level are recorded at an 1 mm interval between the positions of the beam-guide exit and the ion trap. The rotational state and the velocity distributions are extracted from the recorded data.

As pointed out in the previous studies [16,17], there are two competing processes to determine the detection efficiency of the QMS. In short, the ionization efficiency increases with decreasing the longitudinal velocity of the guided molecules, while the detection efficiency of slow molecules decreases due to the increase in beam divergence. In order to consider the latter effect, the molecules outside of the ionization cage ($\phi = 25$ mm) of the ion source are not counted in the present simulation.

B. Comparison of experiment and simulation results for the velocity distributions

The simulation results of the velocity-selected CH_3CN molecules are summarized in Fig. 7. The experimental longitudinal velocity distributions tend to be narrow in comparison to the simulation ones, because the detection efficiency of the slow and the fast velocity components becomes low.

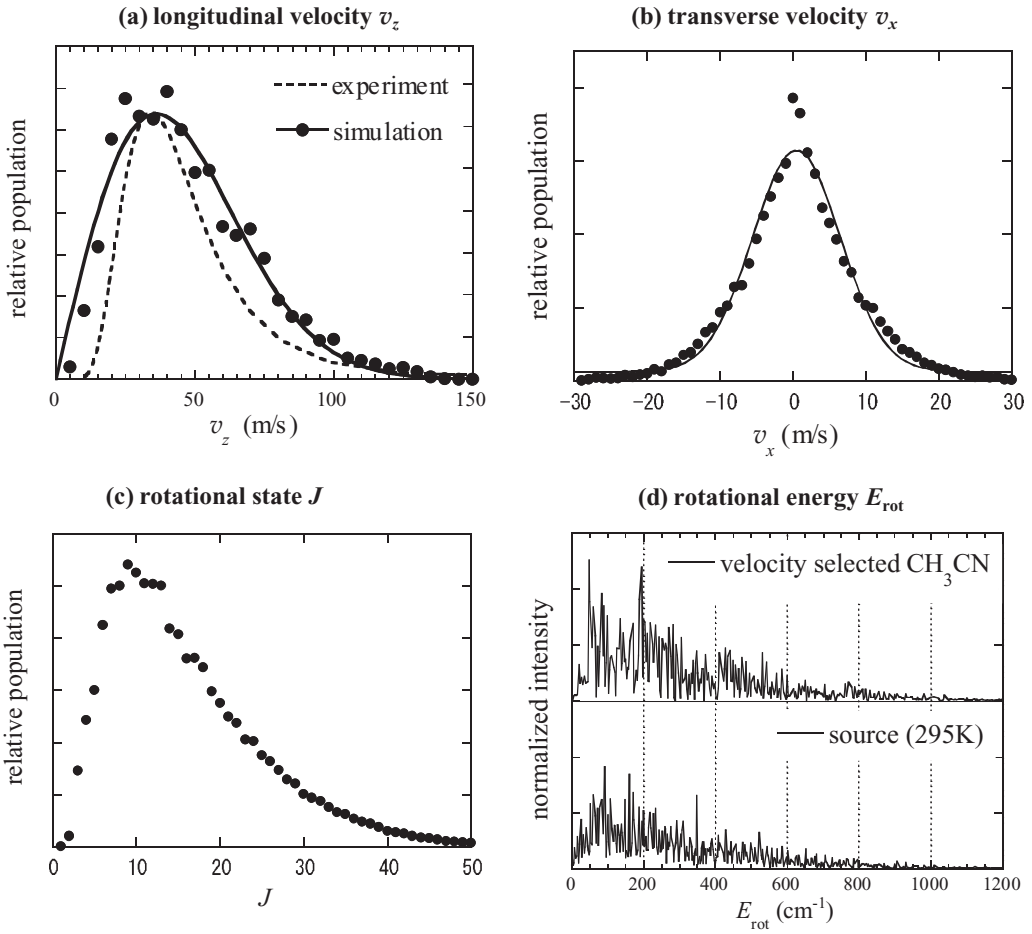

FIG. 7. Results of the Monte Carlo simulation of the velocity-selected CH_3CN. The maximum rotational levels considered is $J_{max} = 50$, and the trial number of the input molecules is 4×10^3 for each rotational level of $|J,K,M\rangle$, where J, K, and M are rotational quantum number, quantum number of component of angular momentum along molecular axis, and projection of $\boldsymbol{J}$ on the fixed axis, respectively. The temperature of the polar gas source is assumed to be 295 K. (a) The longitudinal velocity (v_z) distribution at the center of the ion trap. The dashed line shows the experimental result at $V_G = \pm 3.0$ kV, which is displayed in Fig. 2(b). The solid line is the result of the least-square fit of the one-dimensional thermal velocity distribution function to the simulation result. The most probable velocity of the fitted function is 51(1) m/s. The peak velocity is good agreement with the experimental result. (b) Simulated transverse velocity distribution. The solid curve shows the fitted Gaussian function to the simulated data points. The most probable velocity is 8.5(0.2) m/s, which corresponds to the thermal energy of 178(8) mK. (c) The rotational J-state distribution of velocity-selected CH_3CN. (d) Rotational energy distributions of the velocity-selected CH_3CN and the source gas. In the spectrum of the velocity-selected CH_3CN, the population of the lower energy part is relatively high in comparison to that of the room temperature gas.

Nonetheless, the experimental peak velocities in Fig. 2 are good agreement with the simulation results. Thus, it is possible to characterize the rotational energy distribution as well as the velocity distributions of the velocity-selected polar molecules by using the present simulation results.

First, we evaluated the longitudinal temperature (T_{1D}) of the velocity-selected CH_3CN molecules by the present simulation result. As shown in Fig. 7(a), the most probable velocity of the one-dimensional thermal velocity distribution function is 51(1) m/s, which corresponds to $T_{1D} = 6.5$ K. The same simulations have performed for ND_3 and H_2CO molecules and the results are tabulated in Table I. We also evaluated the temperature of the transverse motion. As shown in Fig. 7(b), the transverse velocity distribution is well reproduced by the Gaussian function, which represents the one-dimensional Maxwell-Boltzmann distribution. The most probable velocity is 8.5(0.2) m/s, which corresponds to the thermal energy of 178(8) mK. Figures 7(c) and 7(d) show the simulated rotational state and the energy distributions. The corresponding energy distributions of the gas source at 295 K is also depicted in Fig. 7(d). The J-state distribution of CH_3CN shifts to the lower J side than that of the source gas. Actually, the population of the lower energy part in the energy spectrum of Fig. 7(d) is relatively high in comparison to that of the room temperature gas.

C. Simulation of the beam divergence

The velocity-selected polar molecules spatially expand due to a lack of the guiding fields by the quadrupole electrodes after the molecules pass through the exit of the beam guide. In order to reproduce this behavior in the simulation, the electric

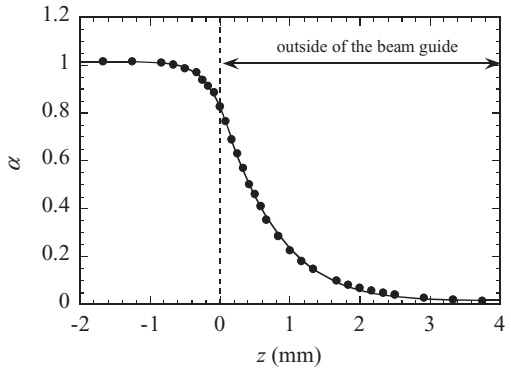

FIG. 8. Numerically calculated normalized geometric factor $\alpha = \kappa(z_i)/\kappa_0$ near the beam-guide exit. At $z = 0$ mm the beam guide is terminated. The solid curve represents the fitted function of Eq. (5) to the calculated points, where we divided two regions of $-2 \leqslant z \leqslant 0.17$ mm and $0.17 \leqslant z \leqslant 5$ mm for the least-square fitting.

fields outside of the beam guide were numerically calculated. First, we calculated the electric potential expressed by

$$\phi(x,y,z) = \frac{\kappa(z)V_G}{r_0^2}(x^2 - y^2), \tag{4}$$

near the beam-guide exit along the z axis using the SIMION 3D code [24]. Then we obtained the geometric factor $\kappa(z_i)$ at different position of z_i as is shown in Fig. 8. The calculated data points are well reproduced by the following function:

$$\kappa(z) = a_1 \exp\{-\exp[-a_2(z + a_3)]\} + a_4, \tag{5}$$

where $a_i (i = 1{-}4)$ are the fitting parameters. Using the potential expressed by Eq. (4), the electric fields outside the beam guide were calculated.

Examples of the simulated beam images at positions near the center of the ion trap are shown in Fig. 9. From the simulated images, the integrated intensity within a 2 mm × 1 mm square at the center, which corresponds to a small central area of the ion trap, is calculated as a function of the position L. As shown in Fig. 10, the intensity gradually decreases

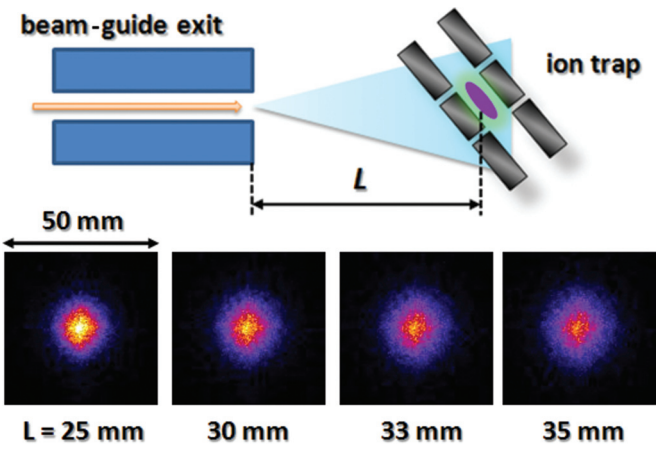

FIG. 9. (Color online) Schematics of the geometry of the beam-guide exit and the ion trap, and the simulation images of velocity-selected CH_3CN molecules near the ion trap center. The simulation parameters are the same as Fig. 7.

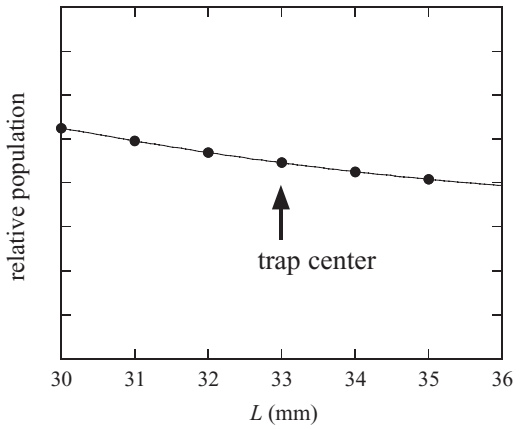

FIG. 10. A plot of the integrated intensity of the CH_3CN molecules within a 2 mm × 1 mm square at the center as a function of the distance L between the beam-guide exit and the detection plane. The trap center is designed to at $L = 33$ mm and the expected uncertainty is ±1 mm. The error of the number density of the velocity-selected CH_3CN by the beam-divergence effect was estimated to be 10%.

with increasing distance from the beam-guide exit. Since the uncertainty of the ion trap position from the beam-guide exit is estimated to be within 2 mm in the present setup, the systematic error of the number density due to the beam divergence is expected to be 10% for CH_3CN, 14% for ND_3, and 22% for H_2CO, respectively.

V. REACTION-RATE MEASUREMENTS

A. Reactions between Ca^+ Coulomb crystal and slow polar molecules

As a first experiment and before starting the reaction-rate measurements between sympathetically cooled molecular ions and velocity-selected polar molecules, the study of the reactivity between polar molecules and a Ca^+ Coulomb crystal was carried out. For this purpose, we performed reaction-rate measurements between a Ca^+ Coulomb crystal and velocity-selected CH_3CN and ND_3. Since the number density of the laser-cooled Ca^+ ions is considered to be constant as a first approximation, the relative number of ions can be determined from the volume of the Ca^+ Coulomb crystal, which can be determined by the size of the observed fluorescence image with the assumption of cylindrical symmetry. In the present measurements, the relative number of Ca^+ ions is measured as a function of reaction time [25].

To begin with, we calculated the energies of the Ca^+-CH_3CN reaction system as shown in Fig. 11(a) [26]. It can be seen that for the ground state $Ca^+(^2S_{1/2})$ only the radiative association (RA) process is possible. However, such a RA process is expected to be very slow under the ultrahigh vacuum conditions of our experiment [27]. On the other hand, the laser-induced reaction, $Ca^+(^2P_{1/2}) + CH_3CN \rightarrow CaH^+ + CH_2CN$, is possible to occur energetically and is the dominant process.

Figure 12(b) shows a plot of the relative number of ions in the Ca^+ Coulomb crystal as a function of time when irradiating with velocity-selected CH_3CN molecules. The

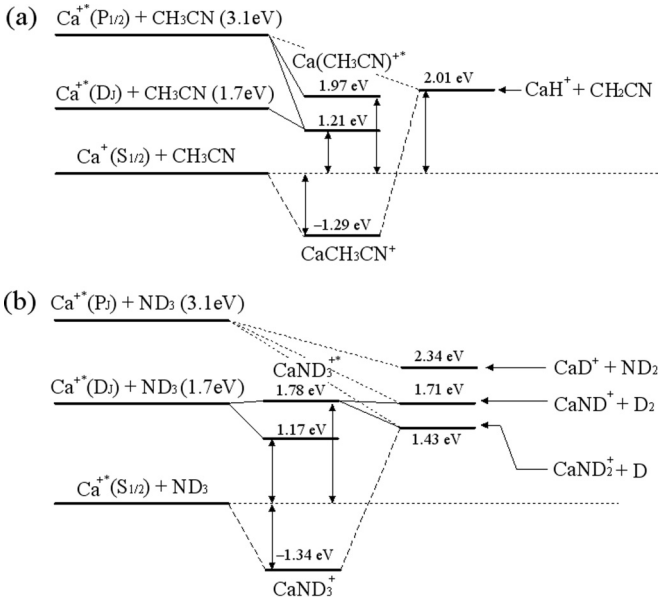

FIG. 11. Energy diagrams of (a) Ca^+-CH_3CN and (b) Ca^+-ND_3 reaction systems calculated by the quantum chemical calculation packages (GAUSSIAN 03) [26]. The geometry optimization of molecular ions and calculations of zero-point energies were performed by B3LYP/6-31G(d). The ground-state energies were calculated using B3LYP/6-311 + (3*df*, 3*pd*) in the optimized geometries. The excited state energy of the association product ion was calculated by the CI-Singles method for the optimized geometry.

average collision energy of this reaction system is estimated to be lower than 10 K by the results of the TOF measurement of the velocity-selected CH_3CN and the molecular dynamics simulation of the Ca^+ Coulomb crystal [14,15]. We also show the corresponding fluorescence images of the Ca^+ Coulomb crystal, which was observed before and after a certain reaction time. A small dark region caused by the product ions was observed in the lower part of the fluorescence image after about one hour reaction time [Fig. 12(b)], where the asymmetric images are considered to be caused by the existence of small asymmetric dc fields in the ion trap [25]. In addition, the crystal became smeared out due to the increase of the number of CaH^+ ions, which slightly heats the Ca^+ crystal.

From these results, it is clear that the observed reaction rate is very slow compared to typical ion–polar-molecule collision rates calculated by the well-known scaling formula [5]:

$$k_t = (0.4767x + 0.62)k_L, \quad x \equiv \mu/\sqrt{2\alpha kT}, \quad x \geqslant 2, \quad (6)$$

where k_L is the Langevin rate, μ is the dipole moment, and α is the polarizability. It is similar to the reaction rate between the background H_2 molecules and the laser-excited $Ca^+(^2P_{1/2})$ ions, where the number density of H_2 was about 2×10^6 cm^{-3} for 10^{-8} Pa [25]. The product CaH^+ ions are also produced by the $Ca^+(^2P_{1/2}) + H_2$ reaction.

The same experiment was performed by irradiating velocity-selected ND_3 molecules to Ca^+ Coulomb crystals. The corresponding energy diagram of the Ca^+-ND_3 reaction system is shown in Fig. 11(b). As with the previous measurement, the laser-excited $Ca^+(^2P_{1/2})$ ions contribute to the reactions. Figure 12(c) shows a plot of the relative number of Ca^+ ions as a function of time when irradiating with velocity-selected ND_3 molecules. As expected from the energy diagram and our previous study [34], the reaction rate of $Ca^+ + ND_3 \rightarrow$ *products* is extremely slow.

TABLE II. Summary of the reaction rate measurements between the velocity-selected polar molecules (CH_3CN, ND_3) and a Ca^+ Coulomb crystal. $\Delta\nu_{uv}$ is the uv laser detuning from the resonance frequency of the $^2S_{1/2}$-$^2P_{1/2}$ transition of Ca^+. The last column shows the initial number of Ca^+ ions estimated by the volume of the Coulomb crystal [15].

$\Delta\nu_{uv}$ [MHz]	γ [s^{-1}]	initial N_{ion}
	(a) without slow polar molecules	
−30	$3.5(1.4) \times 10^{-5}$	1.2×10^3
−40	$2.3(1.6) \times 10^{-5}$	6×10^1
	(b) with slow CH_3CN	
−30	$2.7(0.6) \times 10^{-5}$	5.3×10^3
−40	$1.8(1.0) \times 10^{-5}$	3.3×10^2
	(c) with slow ND_3	
−30	$1.7(1.4) \times 10^{-5}$	1.1×10^3
−30	$3.2(1.1) \times 10^{-5}$	5×10^1
−40	$2.8(1.7) \times 10^{-5}$	3×10^1

A summary of the reaction-rate measurements is shown in Table II. Since the laser-induced reactions depend on the excitation rate of the $^2S_{1/2} \rightarrow {}^2P_{1/2}$ transition of Ca^+, the reaction-rate measurements were performed under different UV laser detunings and ion numbers. As expected, the reaction rates increase with decreasing the laser detuning and the number of ions contained in the Coulomb crystal. However, the differences between these reaction rates are within the mutual errors.

The important conclusion is that the reaction rates measured in the present experiments are very slow compared with typical ion-polar neutral capture rates estimated by Eq. (6). Thus, our results show that reaction-rate measurements of cold molecular ion–polar-molecule reactions can be performed by using a Ca^+ Coulomb crystal, which is used as a coolant to produce various cold molecular ion targets [34].

B. $CH_3CN + N_2H^+ \rightarrow CH_3CNH^+ + N_2$

As an extension of the present experiment, we carried out reaction-rate measurements between sympathetically cooled N_2H^+ ions and the velocity-selected CH_3CN molecules. The reaction system is shown in Fig. 13. Since the system has only one exothermic reaction path, the reaction-rate constant of $CH_3CN + N_2H^+ \rightarrow CH_3CNH^+ + N_2$ can be determined from the decay rate of N_2H^+ ions. The measurement procedure is as follows.

First, we produce a Ca^+ Coulomb crystal in the linear Paul trap, as shown in Fig. 14(a). Then a nitrogen molecular gas of about 1×10^{-7} Pa is introduced into the detection vacuum chamber, and the electron beam is incident to the center of the ion trap in order to produce N_2^+ ions by electron impact ionization. Since the mass of the nitrogen molecular ion is lighter than that of Ca^+, the molecular ions are more tightly bounded by the trapping potential and are accumulated near

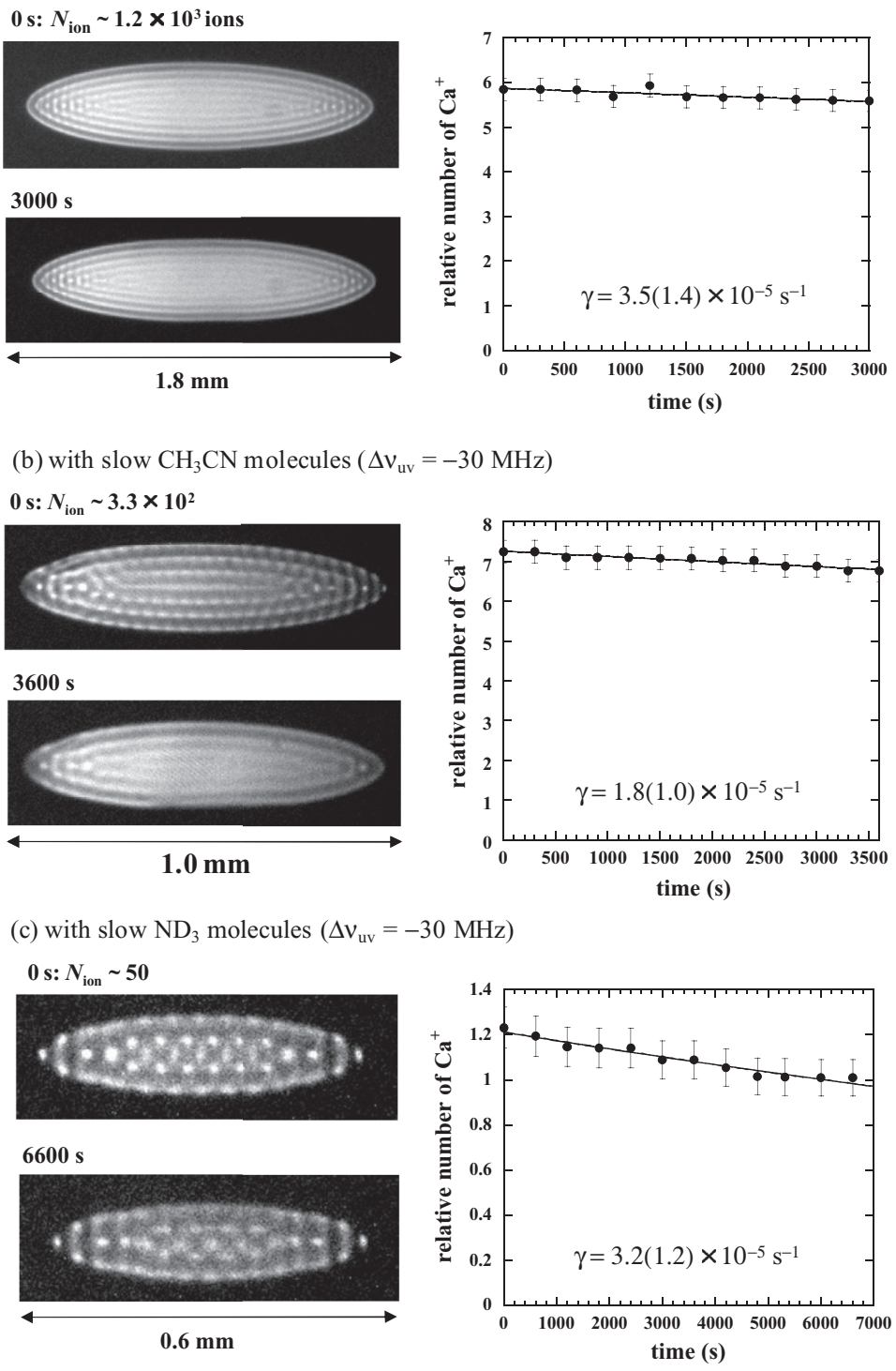

FIG. 12. Examples of the reaction-rate measurements between a Ca^+ Coulomb crystal and the velocity-selected polar molecules (CH_3CN and ND_3). The average collision energy of these measurements is estimated to be lower than 10 K. This is indicated by both the results of the velocity distributions of the polar molecules and the molecular dynamics simulation of the Ca^+ Coulomb crystals [14,15]. The graphs show a plot of the relative number of Ca^+ ions in the Coulomb crystal, which was determined by the size of the observed fluorescence image shown in the left part. (a) A result of the decay rate measurement in a large Ca^+ Coulomb crystal without the velocity-selected polar molecules at a vacuum of 10^{-8} Pa. The ion-molecule reactions between the background H_2 molecules and the laser-excited $Ca^+(^2P_{1/2})$ ions cause the slow decay of the number of Ca^+ ions [25]. (b) A plot of the relative number of the Ca^+ in a small crystal as a function of time when irradiating with velocity-selected CH_3CN molecules. The guiding voltage is set to ±3 kV and the nozzle pressure is 32 mTorr at room temperature. (c) A plot of the relative number of the Ca^+ as a function of time when irradiating with velocity-selected ND_3 molecules. The guiding voltage is set to ±3 kV and the nozzle pressure is 40 mTorr at room temperature.

the trap axis. Finally, an increase of dark area is observed in the fluorescence image after this process [Fig. 14(b)]. It is noted that N^+ ions are also produced by about 20% probability in the ionization process [28]. However, the sympathetic cooling efficiency of the laser-cooled Ca^+ ions is too small to cool the N^+ ions. According to the criterion derived by Baba *et al.* [29], the lighter ions than $0.54m_{LC}$ are heated and finally are lost from the ion trap, where m_{LC} is the mass of the laser-cooled ions.

After the preparation of cold N_2^+ ions, a hydrogen molecular gas of about 6×10^{-6} Pa is introduced into the vacuum chamber. The ion molecule reactions between N_2^+ and H_2 produce only N_2H^+ ions [30]. As shown in Fig. 14(c), the LIF image of the two-species Coulomb crystal becomes smeared out during this process, because the H_2 collisions induce large micromotion amplitudes of Ca^+ ions. From the reaction-rate constant ($k = 2.1 \times 10^{-9}$ cm^3 s^{-1}) at room temperature, we estimated the production rate of N_2H^+ as 3 ions/s.

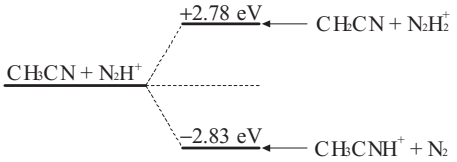

FIG. 13. Energy diagram of the N_2H^+-CH_3CN reaction system calculated by the same method in Fig. 11. The only the exothermic reaction path is proton-transfer reaction, that is, $CH_3CN + N_2H^+ \rightarrow CH_3CNH^+ + N_2$. Although there are other possible endothermic paths, only the lowest endothermic path is depicted.

Since the reaction time is typically 240 s, all of N_2^+ ions change into N_2H^+ ions under the present experimental conditions. As shown in the final image of Fig. 14(d), no significant loss of the molecular ions was observed.

After the preparation of cold N_2H^+ ions, we irradiated the velocity-selected CH_3CN molecules to the two-species Coulomb crystal. Figure 15 shows the snapshots of the LIF images at several reaction times. The dark area progressively decreases with increasing reaction time due to the progress of $CH_3CN + N_2H^+ \rightarrow CH_3CNH^+ + N_2$ reactions. We also observed an increase of the sparse dark area in the outer peripheral region of the Ca^+ Coulomb crystal because a part of the reaction products (CH_3CNH^+) are trapped in the ion trap. In the present experimental conditions, the average reaction energy is estimated to be about 3 K [31].

In order to obtain the reaction rate, we determine the relative number of molecular ions from the volume of the dark area in

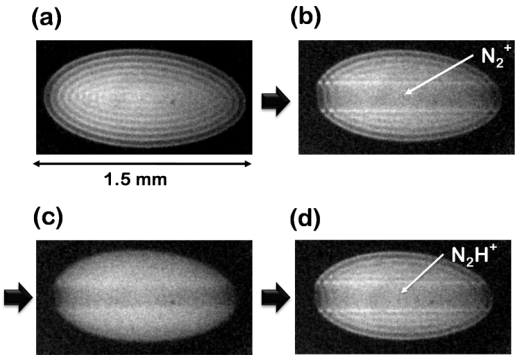

FIG. 14. The production process of cold N_2H^+ ions. (a) Initial state of a Ca^+ Coulomb crystal. The number of Ca^+ is estimated to be about 4×10^3. A nitrogen molecular gas of about 1×10^{-7} Pa is introduced into the vacuum chamber and the electron beam is incident to the ion trap in order to produce nitrogen molecular ions by electron impact ionization. The electron beam energy is set to 250 eV. (b) A two-species Coulomb crystal containing Ca^+ and N_2^+ ions. (c) The LIF image of the two-species Coulomb crystal during the production process of N_2H^+ ions. A hydrogen molecular gas of about 6×10^{-6} Pa is introduced into the vacuum chamber. The ion molecule reactions of $N_2^+ + H_2 \rightarrow N_2H^+ + H$ necessarily produce cold N_2H^+ ions [30]. The image of the two-species Coulomb crystal becomes smeared out because the H_2 collisions heat the Ca^+ ions. (d) The final state of the N_2H^+ production process is reached after four minutes. No significant loss of the molecular ions was observed for this time period.

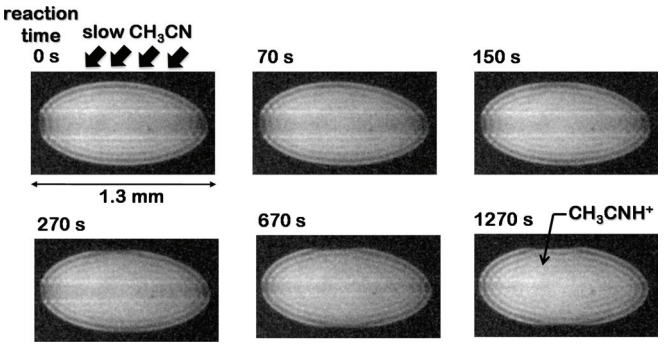

FIG. 15. Sequential LIF images of the two-species Coulomb crystal containing Ca^+ and N_2H^+ during $CH_3CN + N_2H^+ \rightarrow CH_3CNH^+ + N_2$ reactions. The dark area progressively decreases with increasing reaction time. This means that the cold ion-molecule reaction proceeded. As the reactions proceed, the sparse dark area due to the product ions also appears in the outer peripheral region of the Ca^+ Coulomb crystal.

the observed fluorescence images under the assumption of the constant number density at 0 K, which is derived by Poisson's equation under the pseudopotential approximation [25]. We also assume the cylindrical symmetry of the spatial distribution of cold N_2H^+ ions in the early stage of the reaction. Since the number of ions contained in the edge of the ion crystal is expected to be very small on average, it was ignored as a first approximation.

As shown in Fig. 16, there is actually a good correlation between the volumes calculated from the simulation images and the number of N_2H^+ ions as long as there are sufficient number of molecular ions so that the ions extend to both ends of

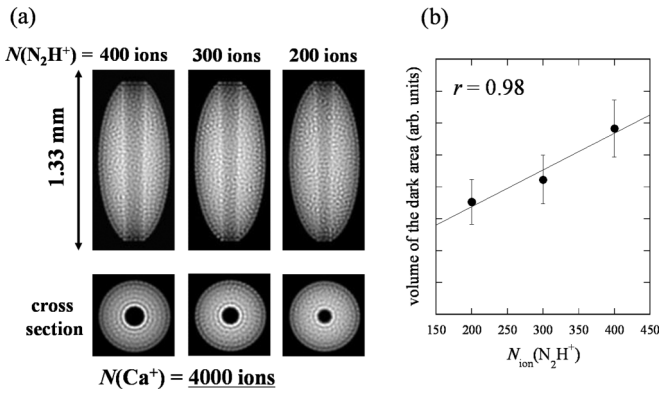

FIG. 16. (a) Simulation images of two-species Coulomb crystal containing 4000 Ca^+ ions and several hundred of N_2H^+ ions. The dark area of the Ca^+ Coulomb crystal is caused by the existence of sympathetically cooled N_2H^+ ions. The simulation method is explained in Refs. [14,15]. The temperature of the virtual light atoms for cooling of Ca^+ is set to 10 mK and the other trapping parameters are set to the same values as the present experimental conditions. (b) A plot of the calculated volume of the dark area as a function of the number of N_2H^+ ions. Each data point is obtained by the square of the averaged horizontal width of the dark area in the simulation images. The error is estimated by the uncertainty of the horizontal width of dark area. The correlation coefficient r is about 0.98. A good correlation is obtained between the volumes and the number of N_2H^+ ions at least in this range.

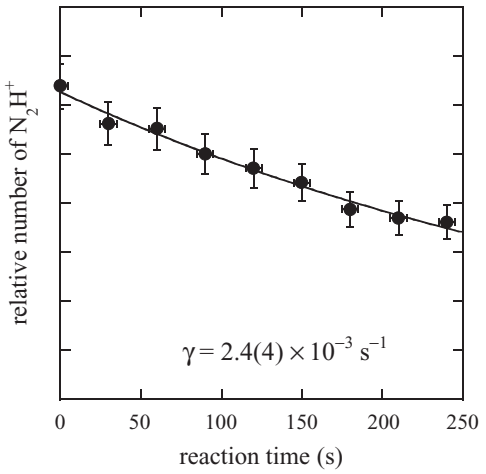

FIG. 17. A plot of the relative number of N_2H^+ ions as a function of the reaction time in $CH_3CN + N_2H^+ \rightarrow CH_3CNH^+ + N_2$. The average reaction energy is estimated to be about 3 K.

the Ca^+ Coulomb crystal. This means that the number density of the sympathetically cooled molecular ions is approximately constant at least on a time average.

Figure 17 shows the decay curve of the relative number of N_2H^+ ions as a function of the reaction time. Each data point was obtained by the square of the averaged vertical width of the dark area in the experimental LIF images. In this example, the reaction rate γ is determined to be $2.4(4) \times 10^{-3}$ s^{-1} by a least-square fit of the exponential function to the data points. The data points up to 240 s in reaction time were used in order to satisfy the above assumptions. Actually we performed nine measurements and obtained the averaged reaction-rate of $2.0(2) \times 10^{-3}$ s^{-1}. The present reaction rate is much faster than those of the reactions between cold Ca^+ and the velocity-selected polar molecules. This is strong evidence that the velocity-selected molecules actually react with the sympathetically cooled N_2H^+ ions. It is noted that the reaction between $N_2H^+ + H_2$ never proceeds further because N_2H^+ ion is a final product of the reaction sequence.

Using the number density of the velocity-selected CH_3CN given in Table I, the preliminary result of the reaction-rate constant is also determined to be $1.7(6) \times 10^{-8}$ cm^3 s^{-1} at the average reaction energy of about 3 K. Although the error caused by the assumptions to obtain the relative number of molecular ions is not included, the main contribution to the error is expected to be the uncertainty of the number density of CH_3CN. The unknown error will be determined from the best-fit simulation image obtained by performing MD simulations of large two-species Coulomb crystals using a computing machine for many-body particle simulations [32]. This issue will be solved in the near future. Nevertheless, the present reaction-rate constant is consistent with the extrapolation value of $k_{RT}\sqrt{T/300} = 4.0 \times 10^{-8}$ cm^3 s^{-1} at about 3 K, where k_{RT} is the experimental rate constant at room temperature [33]. We also estimated the capture rate as $k_{ts} = 3.6 \times 10^{-8}$ cm^3 s^{-1} by the trajectory-scaling formula [5], which is considered to be the maximum value of the reaction-rate constant. In any case, the estimated reaction-rate constants seem to be overestimated by a factor of 2 compared to the present measured reaction-rate constant. Since the reaction path is very simple, it should be possible to precisely compare the experimental rate constant to theoretical values by quantum chemical calculations. This is an interesting issue to be continued and studied in the near future.

VI. SUMMARY AND CONCLUSION

A combined Stark-velocity-filter–ion-trap apparatus has been developed with the aim of future systematic reaction-rate measurements between sympathetically cooled molecular ions and velocity-selected polar molecules. So far we have confirmed the generation of slow ND_3, H_2CO, and CH_3CN molecules having a thermal energy of a few Kelvin by time-of-flight measurements. The number densities of the slow polar molecules were determined to be $n = 10^4$ to 10^6 cm^{-3} at the ion trapping region. Both the reaction temperature and the number density of the collision partners are important parameters to determine the reaction-rate constant of the ion–polar-molecule reactions of interest.

To lead the way, we performed the reaction-rate measurements of $Ca^+ + CH_3CN$ and $Ca^+ + ND_3$ at lower than 10 K. In summary, the reactivity of these slow polar molecules is very low with the Ca^+ Coulomb crystal at low temperatures, and the reaction rates are very slow compared with typical ion-polar neutral reaction rates. Therefore, the loss of the Ca^+ ions is negligible during the proposed reaction rate measurements.

As a first measurement, we performed the reaction-rate measurement between sympathetically cooled N_2H^+ ions and the velocity-selected CH_3CN molecules. Then, the reaction-rate constant at about 3 K was estimated from the measured reaction-rate and the experimentally determined number density of CH_3CN. The result is consistent with the experimental rate constant at 300 K and the calculated value based on the trajectory scaling formula.

In order to perform systematic measurements of interstellar ion chemistry in the near future, various rotationally cold polar molecules and molecular ions will be prepared in our laboratory. Recently, we have demonstrated the sympathetic crystallization of CaH^+ which were produced by laser-induced reactions [25]. In addition, cold $ND_x^+ (x = 2,3)$ ions were also produced after electron impact ionization [34]. Although these cold molecular ions are candidates to measure the reaction rates, the rotational temperatures are still higher than those in interstellar environments (T = 10–100 K). Therefore, the cryogenic ion trap will be further developed to prepare also rotationally cold molecular ions. It is expected to be better to combine the two-color resonance-enhanced-multiphoton ionization technique to prepare state-selected translationally cold molecular ions [35]. On the other hand, the rotationally cold polar molecules are also needed to perform the cold chemical reactions, which actually occur in interstellar clouds. This issue can be solved by using a 4 K cryogenic gas reservoir filled with helium and polar gases for the present Stark velocity filter [12].

ACKNOWLEDGMENTS

This work is financially supported in part by a Grant-in-Aid for Young Scientists (A), and for Challenging Exploratory Research from the Ministry of Education, Culture, Sports, Science and Technology (MEXT), and by the Robert A. Welch Foundation under Grant No. A1546.

[1] E. Herbst and W. Klemperer, Astrophys. J. **185**, 505 (1973).
[2] J. Woodall, M. Agúndez, A. J. Markwick-Kemper, and T. J. Millar, Astrnom. Astrophys. **466**, 1197 (2007).
[3] The Ohio State University Astrophysical Chemistry Group, http://www.physics.ohio-state.edu/~eric/research.html
[4] V. Wakelam, I. W. M. Smith, E. Herbst, J. Troe, W. Geppert, H. Linnartz, K. Öberg, E. Roueff, M. Agundez, P. Pernot, H. M. Cuppen, J. C. Loison, and D. Talbi, Space Sci. Rev. **156**, 13 (2010).
[5] T. Su and W. J. Chesnavich, J. Chem. Phys. **76**, 5183 (1982).
[6] J. Deiglmayr, A. Grochola, M. Repp, K. Mörtlbauer, C. Glück, J. Lange, O. Dulieu, R. Wester, and M. Weidemüller, Phys. Rev. Lett. **101**, 133004 (2008).
[7] R. V. Krems, Phys. Chem. Chem. Phys. **10**, 4079 (2008).
[8] L. Scharfenberg, S. Y. T. van de Meerakker, and G. Meijer, Phys. Chem. Chem. Phys. **13**, 8448 (2011).
[9] L. Scharfenberg, K. B. Gubbels, M. Kirste, G. C. Groenenboom, A. van der Avoird, G. Meijer, and S. Y. T. van de Meerakker, Eur. Phys. D **65**, 189 (2011).
[10] S. A. Rangwala, T. Junglen, T. Rieger, P. W. H. Pinkse, and G. Rempe, Phys. Rev. A **67**, 043406 (2003).
[11] H. Tsuji, Y. Okuda, T. Sekiguchi, and H. Kanamori, Chem. Phys. Lett. **436**, 331 (2007).
[12] L. D. van Buuren, C. Sommer, M. Motsch, S. Pohle, M. Schenk, J. Bayerl, P. W. H. Pinkse, and G. Rempe, Phys. Rev. Lett. **102**, 033001 (2009).
[13] S. Willitsch, M. T. Bell, A. D. Gingell, S. R. Procter, and T. P. Softley, Phys. Rev. Lett. **100**, 043203 (2008).
[14] K. Okada, K. Yasuda, T. Takayanagi, M. Wada, H. A. Schuessler, and S. Ohtani, Phys. Rev. A **75**, 033409 (2007).
[15] K. Okada, M. Wada, T. Takayanagi, S. Ohtani, and H. A. Schuessler, Phys. Rev. A **81**, 013420 (2010).
[16] T. M. Bell, A. D. Gingell, J. M. Oldham, T. P. Softley, and S. Willitsch, Faraday Discuss. **142**, 73 (2009).
[17] T. Junglen, T. Rieger, S. A. Rangwala, P. W. H. Pinkse, and G. Rempe, Eur. Phys. J. D **31**, 365 (2004).
[18] M. Bart, P. W. Harland, J. E. Hudson, and C. Vallance, Phys. Chem. Chem. Phys. **3**, 800 (2001).
[19] NIFS AMDIS-Molecules Database, http://dbshino.nifs.ac.jp/
[20] V. Tarnovsky *et al.*, Int. J. Mass Spectrom. Ion Processes **167/168**, 69 (1997).
[21] M. Vinodkumar, K. N. Joshipura, C. Limbachiya, and N. Mason, Phys. Rev. A **74**, 022721 (2006).
[22] C. H. Townes and A. L. Schawlow, *Molecular Spectroscopy* (Dover, Mineola, 1975).
[23] T. D. Hain, R. M. Moision, and T. J. Curtiss, J. Chem. Phys. **111**, 6797 (1999).
[24] SIMION 3D Version 8.0, Scientific Instrument Services Inc., Idaho National Laboratory.
[25] N. Kimura, K. Okada, T. Takayanagi, M. Wada, S. Ohtani, and H. A. Schuessler, Phys. Rev. A **83**, 033422 (2011).
[26] M. J. Frisch *et al.*, software package: GAUSSIAN 03, Revision B.01 (Gaussian Inc., Pittsburgh, 2003).
[27] D. R. Bates, Astrophys. J. **270**, 564 (1983).
[28] A. Crowe and J. W. McConkey, J. Phys. B **6**, 2108 (1973).
[29] T. Baba and I. Waki, Appl. Phys. B **74**, 375 (2002).
[30] D. Smith, N. G. Adams, and T. M. Miller, J. Chem. Phys. **69**, 308 (1978).
[31] The micromotion temperature of N_2H^+ ions is estimated by molecular dynamics simulations under time-dependent rf fields. Since the temperature is estimated to be lower than 1 K, the maximum temperature was applied in order to estimate the average reaction energy. For the velocity-selected CH_3CN, $T_{1D} = 6.4$ K in Table I was applied.
[32] A. Kawai, T. Fukushige, and J. Makino, arXiv:astro-ph/9905101; J. Makino, Publ. Astron. Soc. Jpn. **43**, 621 (1991).
[33] G. I. Mackay, D. Betowski, J. D. Payzant, H. I. Schiff, and D. K. Bohme, J. Phys. Chem. **80**, 2919 (1976).
[34] K. Okada, N. Kimura, T. Suganuma, K. Shiina, T. Furukawa, T. Takayanagi, M. Wada, and H. A. Schuessler, J. Phys. Conf. Ser. **388**, 102001 (2012).
[35] X. Tong, A. H. Winney, and S. Willitsch, Phys. Rev. Lett. **105**, 143001 (2010).